Journal of Translational Medicine

RESEARCH

Open Access

N6-methyladenosine RNA modified BAIAP2L2 facilitates extracellular vesicles-mediated chemoresistance transmission in gastric cancer

Yuhan Liao[1,2†], Xinhua Chen[3†], Hao Xu[1,2†], Yunfei Zhi[4], Xinghua Zhuo[1,2], Jiang Yu[3*] and Liang Zhao[1,2*]

Abstract

Background Extracellular vesicles (EVs) produced in the tumor microenvironment in response to chemotherapy promote chemotherapy-resistant phenotypes. However, the role of EVs proteins induced by gastric cancer (GC) cell chemotherapy in regulating chemotherapy resistance remains unclear.

Methods Immunohistochemistry was used to verify the relationship between brain-specific angiogenesis inhibitor 1-associated protein-2-like protein 2 (BAIAP2L2) expression and chemotherapy resistance in advanced GC. The relationship between BAIAP2L2 and chemotherapy resistance was verified using a subcutaneous tumor model in nude mice. Transmission electron microscopy, nanoparticle tracking analysis, and western blotting were performed to detect purified EVs. Tandem mass tag (TMT) analysis was used to detect differential labels. The interaction between YTH domain-containing family protein1 (YTHDF1) and BAIAP2L2 in GC cells was confirmed by RIP-qPCR analysis using a YTHDF1-specific antibody.

Results We found that BAIAP2L2 was associated with chemotherapy resistance to GC in clinical samples and was increased in chemotherapy-resistant GC cells. Mechanistically, BAIAP2L2 promotes the transfer of chemotherapy resistance from resistant GC cells to sensitive cells through EVs proteins, such as ANXA4. Furthermore, ANXA4 promoted platinum-based chemical resistance in GC by mediating autophagy. Interestingly, YTHDF1 facilitates the translation of BAIAP2L2 and ANXA4 through m^6A modifications.

Conclusions Our findings reveal the key role of BAIAP2L2 as a potential prognostic marker and therapeutic target for chemotherapy resistance in GC.

Keywords Gastric cancer, BAIAP2L2, M^6A, YTHDF1, Extracellular vesicles, Chemoresistance

†Yuhan Liao, Xinhua Chen and Hao Xu have contributed equally to this work.

*Correspondence:
Jiang Yu
balbcyujiang@163.com
Liang Zhao
liangsmu@foxmail.com
Full list of author information is available at the end of the article

Introduction

Gastric cancer (GC) is the fourth most common cancer worldwide. In northeast Asia, the incidence and mortality rates of GC are the highest worldwide [1, 2]. Surgical treatment does not improve patient prognosis; thus, comprehensive adjuvant drug treatment is needed for patients with GC. Although precision therapy, such as HER2-targeted therapy and immune checkpoint inhibitors, can prolong the survival time of some patients with GC [3], platinum-based chemotherapy is still used as the basis for treatment [4]. Therefore, resistance to platinum-based chemotherapy in GC seriously affects the survival of patients with advanced GC.

Brain-specific angiogenesis inhibitor 1-associated protein-2-like protein 2 (BAIAP2L2), also known as BAI1-associated protein-2-like 2, is located on chromosome 22q13.1. The I-BAR family of proteins, including BAIAP2L2, BAIAP2L1(IRTKS), IRSp53, MIM, and ABBA, have been shown to be involved in the regulation of cell membrane formation [5, 6]. BAIAP2L2 promotes the formation of flat or slightly curved membranes, and endogenous BAIAP2L2 proteins are located in the plasma membrane at intracellular vesicles and junctions [6]. BAIAP2L2 promotes the proliferation and growth of lung cancer cells, participates in the development of human osteosarcoma, and promotes tumorigenesis and malignancy in prostate cancer cells [7, 8]. BAIAP2L2 is highly expressed in human gastric cancer tissues and promotes proliferation and metastasis of gastric cancer cells [9]. However, whether BAIAP2L2 is involved in chemotherapy resistance in GC has not been reported.

Extracellular vesicles (EVs) are vesicles with a diameter of 30–200 nm that are released after fusion of intracellular vesicles with the plasma membrane. They are rich in various proteins, nucleic acids, and other important substances and are released in a variety of different cell types. EVs act as a bridge between cells and the microenvironment through vehicle delivery of vehicles [10]. EVs secreted by tumor cells have been shown to promote the proliferation, invasion, and metastasis of tumor cells, inhibit immune responses, and increase the resistance of tumor cells to chemotherapy [11, 12]. At present, most studies on tumor EVs have focused on RNA in EVs [11, 13, 14]. However, an increasing number of researchers are focusing on the function of proteins in EVs and applying proteomic methods to study them [12, 15, 16]. We screened the protein components of EVs in the growth environment of gastric cancer cells related to the progression of platinum-based chemotherapy resistance and studied the mechanisms of chemotherapy resistance. Thus, real-time monitoring and reversal of chemotherapy resistance in gastric cancer can be achieved.

M^6A modification is one of the most important and common messenger RNA modifications that exert influential effects on mRNA splicing, stability, and translation. Recent studies have demonstrated that N6-methyladenosine (m^6A) modification of mRNA plays an important role in GC [17, 18]. METTL3 is upregulated in GC and promotes epithelial-mesenchymal transition (EMT) and metastasis of GC by m^6A modification of zinc finger MYM-type containing 1 (ZMYM1), leading to ZMYM1-mediated repression of the E-cadherin promoter [18]. The YTH domain-containing family protein 1 (YTHDF1), an $m6^A$ reader, plays a crucial role in gastric carcinogenesis. YTHDF1 can promote gastric carcinogenesis via Wnt receptor frizzled7 (FZD7) and USP14 [17], and its loss in gastric tumors restores sensitivity to antitumor immunity by recruiting mature dendritic cells [19].

Here, we aimed to determine the role of BAIAP2L2 as a potential prognostic marker and therapeutic target for chemoresistance in GC. We demonstrated that BAIAP2L2 is overexpressed in GC tissues and promotes the proliferation of GC cells as an oncogenic factor. In addition to the intrinsic effects of BAIAP2L2 on tumor cells, we also revealed that BAIAP2L2 mediates the transmission of chemotherapy resistance in GC cells by regulating EVs proteins and that YTHDF1 can regulate its expression. These data suggest that targeting BAIAP2L2 may be a novel strategy for restoring sensitivity to chemotherapy in GC patients.

Materials and methods

Patient samples

This study was approved by the Institutional Review Board of Nanfang Hospital, Southern Medical University (NFEC-2023–545). We collected samples from GC patients receiving platinum-based chemotherapy before surgery at Nanfang Hospital for protein expression of BAIAP2L2 and YTHDF1, measured by immunohistochemistry (IHC) staining between 2013 and 2023 (n = 78). According to the grade of postoperative tumor regression (TRG), the patients were divided into resistant (n = 53) and sensitive (n = 25) groups. The CAP-TRG grading system is used to evaluate the therapeutic effect of neoadjuvant chemotherapy in gastric cancer. This system classifies the response as follows: TRG0 indicates no viable tumor cells, representing a complete response; TRG1 signifies the presence of single cells or small clusters of residual tumor cells, indicating a partial response; TRG2 reflects the presence of residual tumor cells exceeding fibrosis, indicating a minimal response; and TRG3 denotes few or no tumor cell death, with extensive residual cancer cells, indicating a poor response. For stratification, patients are categorized into sensitive and resistant groups based on the CAP-TRG grading, with

TRG0-2 being classified as the sensitive group and TRG3 as the resistant group.

Cell lines and cell culture

A series of GC cell lines (MKN45 and AGS) were obtained from Foleibao Biotechnology Development (Shanghai, China), and MKN45/DDP Cisplatin resistant cells (MKN45/DDP) were purchased from Meisen CTCC (CTCC-0520-NY, Hangzhou, China). MKN45 cells, extracted from a 62-year-old woman, are a cell line commonly used in gastric cancer studies, and MKN45/DDP were generated based on the resistance induced by long-term exposure to Cisplatin. The initial concentration used to generate resistance started at 1 μM, followed by a dose escalation protocol with a gradient of 0.25–0.5 μM. Each concentration was maintained until cell proliferation stabilized and was passaged for three generations, ultimately reaching a final concentration of 6 μM. Engineered cell line 293 T was purchased from the Cell Bank of Type Culture Collection of the Chinese Academy of Sciences (Shanghai, China) and maintained according to the aforementioned methods [20]. All cell lines were cultured in RPMI 1640 medium (KeyGEN BioTECH, Jiangsu, China) supplemented with 10% fetal bovine serum (FBS) (Gibco-BRL, Invitrogen, Paisley, UK). Cells were maintained in a humidified atmosphere containing 5% CO2 at 37 °C. All cell lines used in this study tested negative for mycoplasma and were authenticated by short tandem repeat (STR) profiling within four years. The STR profiling of MKN45 cells is provided in Supplementary Material 1. All cell line experiments were performed within six months of thawing or cell collection. Cells were transfected with plasmid vectors using Lipofectamine® 3000 reagent (Thermo Fisher Scientific, USA) according to the manufacturer's protocol.

RIP-qPCR and MeRIP-qPCR

GC cells were harvested and resuspended in IP lysis buffer. After incubation on ice for 30 min, the lysate was collected by centrifugation at 12,000 g for 10 min. Antibodies or pre-immune IgG was added to the lysate, followed by overnight incubation at 4 °C. After washing the beads twice, RNA extraction and qPCR analyses were performed, as described in Supplementary Materials.

Isolation of EVs from cell culture media

We used fresh supernatants from MKN45/DDP cultured in 15 cm dishes for 48 h (EV-depleted medium), with a cell density of 70–80% and a number of 1.4×10^7. MKN45/DDP cell culture media were harvested and centrifuged at 300×g and 3,000×g to remove cells and debris. Subsequently, the supernatant was centrifuged at 10,000×g for 30 min to discard larger shedding vesicles. Finally, the supernatant was centrifuged at 110,000×g for 70 min, and EVs were contained in the pellet, which was resuspended in 1×PBS and filtered through 0.2-μm filters. All steps were performed at 4 °C.

Transmission electron microscopy

Fifteen μL EV samples were absorbed using a pipette gun and placed on copper mesh for 1 min. The EV samples on the copper web were sucked dry with filter paper, and 15 μL of 2% uranyl acetate staining solution was absorbed using a pipette and stained for 1 min at room temperature. The EV samples on the copper mesh were dried using a filter paper, and the dyed samples were roasted under a lamp for 10 min, observed, photographed, and photographed.

Nanoparticle tracking analysis (NTA)

The sample pool was then cleaned with ultrapure water. The instrument was calibrated using polystyrene microspheres (100 nm). The sample pool was then cleaned with 1×PBS. The samples were diluted with 1×phosphate-buffered saline (PBS) and injected for detection.

PKH67 staining

The PKH67 Green Fluorescent Cell Linker Kit (Sigma-Aldrich) is used for lipid bilayer labeling and is widely used as a specific EV dye [21]. The EVs (10 μg/mL) were resuspended in 100 μL of diluent C. A dye solution (4×10−6 M) was prepared by adding 0.4 μL of PKH67 ethanolic dye solution to 100 μL of diluent C. The 100 μL EV suspension was then mixed with 100 μL of dye solution by pipetting (EV group). After incubating the cell/dye suspension for 1–5 min with periodic mixing, staining was stopped by adding 200 μL serum and incubating for 1 min. Stained EVs were washed twice with 1×PBS and resuspended in fresh sterile conical polypropylene tubes. Finally, 10 μg of stained EVs (EV group), 1 ml of PBS solution (without EVs group), or 100 μL of PKH-67 dye solution resuspended in 900 μL PBS solution (PKH only group) were added to the cell medium and incubated for 6 h before imaging, with the number of cells conditioned is 5*10^5.

Tandem mass tags (TMT) analysis of EVs

1. Sample Preparation: Total protein was extracted from cell samples and quantified using the BCA method. The protein samples were precipitated with acetone, and the resulting protein pellets were resolubilized. Disulfide bonds were reduced with dithiothreitol, followed by alkylation with iodoacetamide. Trypsin was added to the samples at a trypsin-to-protein ratio of 1:50 for protein hydrolysis. Subsequently, the trypsin-

to-protein ratio was adjusted to 1:5 for further digestion of the protein samples.

2. Peptide Digestion: Each sample was labeled using the TMT isobaric labeling reagent set (Thermo Fisher Scientific, Rockford, USA), and labeled samples within each group were mixed in equal proportions. The resulting peptide samples were desalted, lyophilized, and redissolved in mobile phase A before separation under alkaline conditions using RP-UPLC. For each sample, 2 μg of the mixture was analyzed by mass spectrometry to assess the labeling efficiency of each TMT-labeled mixture, with TMT (N-terminal/K) as variable modifications. The labeling efficiency, calculated as the ratio of the number of TMT-labeled sites to all potential labeling sites, was required to exceed a 95% threshold before proceeding to the separation step.
3. LS-MS/MS Analysis: Samples were analyzed using an Orbitrap Fusion Lumos Tribrid mass spectrometer equipped with a nanospray ion source and a nano-liquid chromatography (nano-LC) system (Thermo Fisher, San Jose, CA, USA). Data acquisition was performed on a Q Exactive HF-X mass spectrometer coupled with the Easy-nLC 1200 system (both from Thermo Scientific).
4. Data Analysis: Raw data files were analyzed using Proteome Discoverer 2.2 software (Thermo Fisher Scientific, USA). Searches were performed against the UniProt human database (Uniprot-Human-Jan 15, 2018.fasta.sequest HT) to identify peptide fragments, with precursor and fragment mass tolerances set to 10 ppm and 0.6 Da, respectively. Fully tryptic peptides with up to two missed cleavages were accepted. Search results were filtered at the peptide spectrum match level using a strict false discovery rate (FDR) q-value of 0.01 and a relaxed FDR q-value of 0.05. GO pathway enrichment analysis was conducted using the BGI online analysis system, Dr. Tom. Venn diagrams and heatmaps were generated using OmicStudio tools on the open platform (https://www.omicstudio.cn). A fold change > 2.0 and p-value < 0.05 were set as the cutoff criteria. The table of all proteins identified through the TMT proteomics analysis was shown in Supplementary material 2.

Bioinformatics

Public bulk RNA-seq data were downloaded from the The Cancer Genome Atlas (TCGA) datasets (http://cancergenome.nih.gov/) and The UCSC Xena project (http://xena.ucsc.edu). Differential expression analysis based on the expression count matrix was performed using R package limma [22]. The genes that simultaneously met the threshold of |log2 Fold Change| > 1.5 and p-value < 0.05 by limma were identified as convincing differentially expressed genes (DEGs). Univariate Cox analysis was performed to identify the genes associated with prognosis (PAGs) via the R package survival. Kaplan–Meier curves of candidate genes were drawn based on GEPIA2 [22].

To interpret the bulk RNA-seq data comprehensively, functional and pathway enrichment analyses were performed using diverse database resources, including the Kyoto Encyclopedia of Genes and Genomes (KEGG) pathways [23] and Gene Ontology (GO) database [24]. Two principal approaches, over-representation analysis (ORA) and gene set enrichment analysis (GSEA), were used for the analyses. The aforementioned analyses were performed using the R package ClusterProfiler [25].

A volcano plot was constructed to identify differentially expressed proteins in EVs. Hierarchical clustering was performed to identify protein clusters. GO annotation was performed to identify gene regulatory networks based on hierarchical categories according to molecular function, biological process, and cellular component terms. Pathway analysis was performed with the Kyoto Encyclopedia of Genes and Genomes (KEGG) (http://www.genome.jp/kegg/ and https://david.ncifcrf.gov/) to characterize the enriched pathways.

In addition, the TIMER2.0 database [26] was used to evaluate the correlation between target gene and mRNA methylation.

Statistical analyses

The figures and graphical elements in this manuscript were created and compiled using Figdraw (https://www.figdraw.com/) and Adobe Illustrator 2023 (Adobe, San Jose, CA, USA). The results were analyzed using SPSS statistical software (version 24.0; SPSS, Inc., Chicago, IL, USA) and GraphPad Prism 8 software (GraphPad Software, Inc., CA, USA). Statistical tests included Student's t-tests (paired or unpaired), one-way analysis of variance (ANOVA), Pearson correlations, Pearson's chi-squared test (χ^2), and Kaplan–Meier analysis. Statistical significance was set at $P < 0.05$. * $P < 0.05$, ** $P < 0.01$, *** $P < 0.001$, ns not significant.

Results

Screening potential targets for platinum-based chemotherapy resistance in gastric cancer based on public databases

The workflow shows how we identified five genes (BAIAP2L2, TRIM15, TRIM29, KRTCAP3, and GPR35) and pathways associated with gastric cancer progression and chemotherapy resistance, based on differential expression analysis, cox survival analysis, and GSEA

analysis (Fig. 1A). The data of 408 tumor tissues and 36 normal tissues were extracted from TCGA database and used for limma-based differential expression analysis to obtain tumor-specific genes highly expressed in tumors (n = 1219, Fig. 1B). Differential expression analysis was used to identify the genes associated with platinum drug resistance. In view of the obvious differences in the use of different platinum drugs in clinical practice, to ensure the reliability of the analysis, we only extracted the data of patients receiving cisplatin chemotherapy from TCGA database (n = 48) and divided the patients into sensitive and resistant groups according to whether they relapsed. Finally, 217 genes were found to be upregulated in cisplatin-resistant genes (Fig. 1C). Survival and univariate

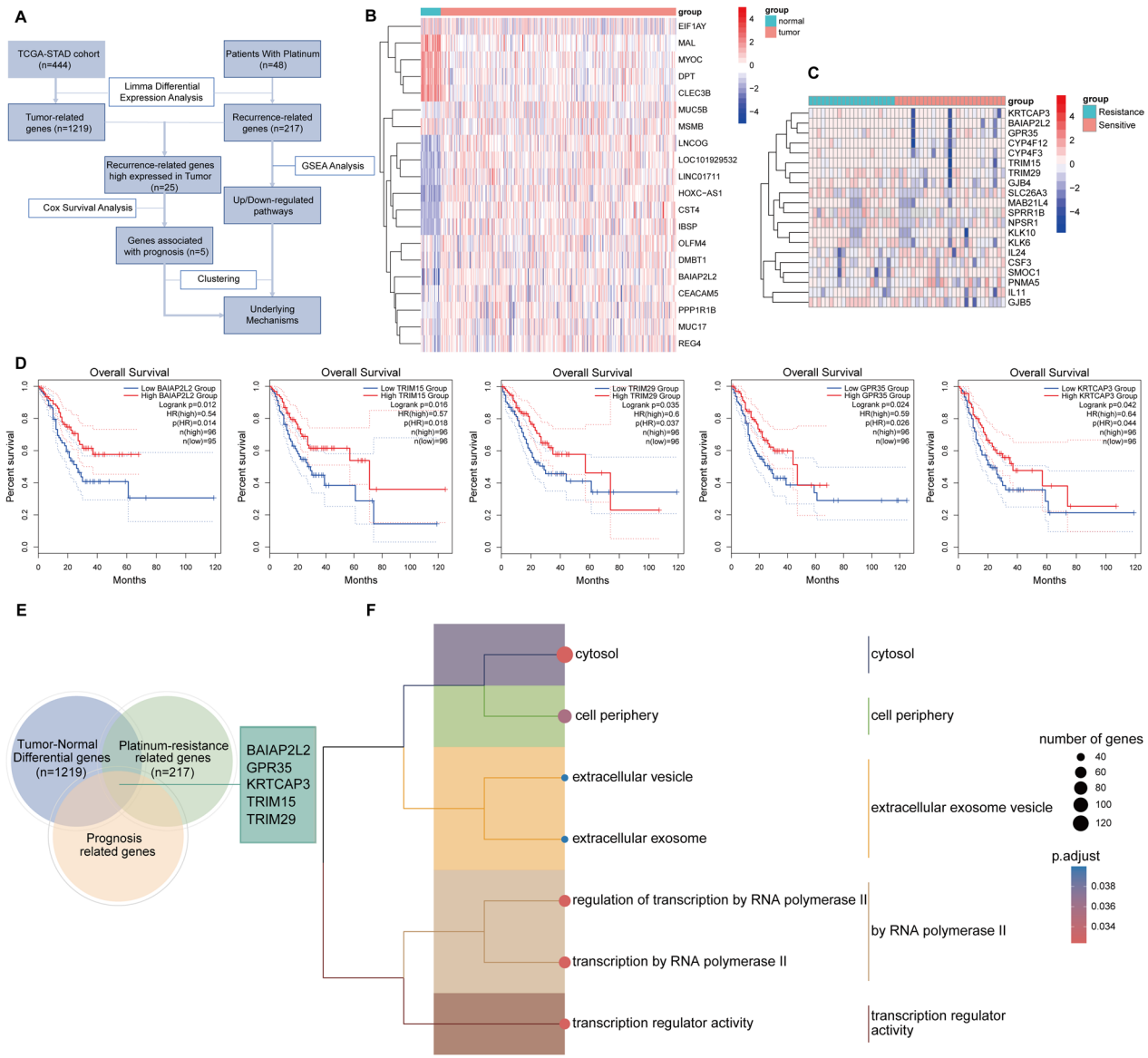

Fig. 1 Screening potential targets for platinum-based chemotherapy resistance in gastric cancer based on public databases. **A** The flowchart of the screening process of BAIAP2L2. **B** Differential expression analysis between normal and tumor tissues which were extracted from the TCGA database. **C** Differential expression analysis between relapse group and non-relapse group which was grouped by whether relapse after receiving cisplatin-based chemotherapy. **D** Survival analysis, including univariate Cox analysis and K-M method, indicated that BAIAP2L2 was relatively prominent among the cisplatin recurrence related genes highly expressed in tumors correlated with prognosis. **E** Candidate genes were the intersection of differential expression analysis between normal and tumor, relapse and non-relapse, and survival analysis. **F** The treemap via GO analysis for possible mechanism of cisplatin recurrence in gastric cancer mining with the 25 cisplatin recurrence related genes highly expressed in tumors

Cox analyses were used to further evaluate these genes, five of which were found to be associated with prognosis. Kaplan–Meier analysis was used to plot the survival curves of these five genes, with BAIAP2L2 being relatively prominent (Fig. 1D). After intersection of the above two differential analyses (Fig. 1A, B), 25 genes were identified as cisplatin recurrence-related genes that were highly expressed in tumors. To explore the possible mechanism of cisplatin recurrence in gastric cancer, we performed GO database-based enrichment analysis based on these 25 genes (Fig. 1E, F). Several pathways were enriched to be associated with resistance, including RNA polymerase II, extracellular vesicles, and extracellular EVs, which were regulated in the drug resistance group.

BAIAP2L2 up-regulation promotes platinum-based chemoresistance in GC

QPCR showed that the expression of BAIAP2L2 in cis-platinum (DDP)-resistant GC cells was significantly higher than that in DDP-sensitive cells. However, TRIM15, TRIM29, KRTCAP3, and GPR35 did not show as significant difference as BAIAP2L2 in qPCR results (Fig. 2A). Western blot also confirmed that the expression of BAIAP2L2 was significantly higher in DDP-resistant GC cells compared to DDP-sensitive cells (Fig. 2B). Western blot result confirmed that the knockdown of BAIAP2L2 was achieved (Fig. 2C). Moreover, the CCK-8 assay confirmed that BAIAP2L2 significantly increased resistance to platinum chemotherapeutics in GC cells (Fig. 2D–F and Fig. S1). Subsequently, we knocked down BAIAP2L2 expression in chemotherapy-resistant GC cells (MKN45/DDP) and performed a subcutaneous tumor xenograft experiment in BALB/c Nude mice. On the day of dissection, the weight and volume of the subcutaneous tumors formed by BAIAP2L2 knockdown cells were smaller than those formed by control cells (Fig. 2G and H). We collected 78 gastric cancer samples from patients receiving platinum-based chemotherapy in our clinical cohort. IHC staining showed that the expression of BAIAP2L2 in GC tissues of patients resistant to platinum-based treatment was significantly higher than that in the sensitive group (Fig. 2I, J). These data indicated that BAIAP2L2 contributes to platinum-based chemoresistance in GC cells.

Chemotherapy resistant GC cells transmit chemotherapy resistance to sensitive cells through EVs

Several pathways including extracellular vesicles and EVs were enriched (Fig. 1F). GSEA analysis to identify the cisplatin resistance-related pathways that BAIAP2L2 may participate in, indicated that the cell periphery, cytoplasm, extracellular vesicles, and plasma membrane were mainly involved in the cisplatin resistance process (Fig. 3A). To confirm whether EVs derived from chemotherapy-resistant GC cells (EVs_MKN45/DDP) played a key role in the development of drug resistance, we first isolated EVs from the conditioned media of resistant GC cells. The purified EVs appeared as small, round vesicles with diameters were 30–200 nm (Fig. 3B, C). HSP70, TSG101, and CD9 were expressed in the EVs, and we have shown an additional marker (CD63) that is negligible in EVs compared to cells, with the EV protein used for Western Blot was 10 μg (Fig. 3D). Furthermore, MKN45 cells were incubated with PKH67-labeled EVs (10 μg/mL) isolated from MKN45/DDP conditional medium or with PKH67 dye alone (without EVs) under the same labeling conditions, and fluorescent labeling revealed that EVs_MKN45/DDP45 was internalized by the sensitive MKN45 cells (Fig. 3E, F). MKN45 cells were incubated with EVs purified from MKN45/DDP cells for 24 h, followed by treatment with DDP for an additional 24 h to assess the potential transfer of drug resistance. To ensure that the observed effects were specifically mediated by EV transfer, the negative control for resistance transfer consisted of recipient cells treated with conditioned media from resistant cells depleted of EVs. The CCK-8 assay showed that co-culture with EVs_MKN45/DDP (20 μg/mL) significantly increased the resistance of MKN45 cells to chemotherapy. After co-culture with EVs isolated from MKN45/DDP which treated with EV inhibitor GW4869, MKN45 cells were more sensitive to chemotherapy than before the treatment of GW4869 with MKN45/DDP (Fig. 3G). These data revealed the transfer of chemotherapy resistance from chemotherapy-resistant GC cells to chemotherapy-sensitive cells through EVs (mechanism overview diagram, Fig. 3H).

BAIAP2L2 promotes the transfer of chemotherapy resistance from resistant GC cells to sensitive cells through EVs.

Purified EVs (20μL) from knockdown or control BAIAP2L2 MKN45/DDP cells appeared as small, round vesicles with diameters were 30–200 nm (Fig. 4A). Subsequently, NTA showed that the proportion and concentration of isolated EVs from conditioned media of BAIAP2L2 knockdown-resistant GC cells were lower in the diameter range of 30–200 than in the control group (Fig. 4B). Furthermore, IF revealed that a larger quantity of EVs was isolated from resistant cells and internalized by sensitive MKN45 cells when overexpress BAIAP2L2 in MKN45/DDP (Fig. 4C, D). Moreover, we tested the expression of EV markers (HSP70, TSG101, CD9 and CD63) and BAIAP2L2 in knocked-down or control BAIAP2L2 MKN45/DDP cell proteins and corresponding EVs were analyzed by Western Blot (Fig. 4E). The CCK-8 assay confirmed that co-culture with EVs (20 μg/mL)

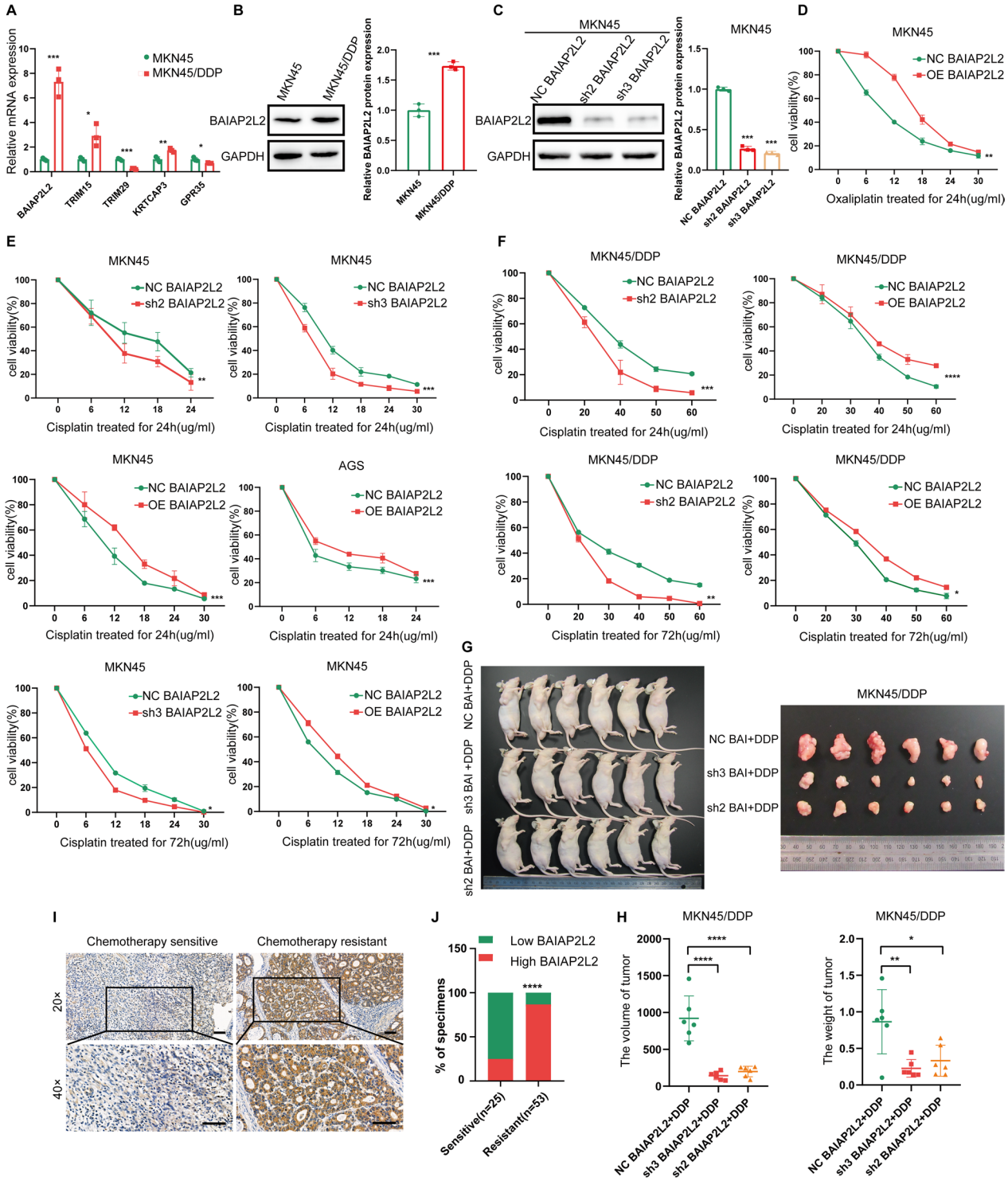

Fig. 2 BAIAP2L2 up-regulation promotes platinum-based chemoresistance in GC. **A** qPCR showed the expression of BAIAP2L2, TRIM15, TRIM29, KRTCAP3 and GPR35 in DDP-resistant GC cells and DDP-sensitive cells. **B** Western Blot showed the expression of BAIAP2L2 in DDP-resistant GC cells and DDP-sensitive cells. **C** Western blot confirmed BAIAP2L2 was knocked down. **D-F** CCK-8 were used to explore the effect of BAIAP2L2 on the resistance to platinum chemotherapeutics of GC cells. Data of CCK-8 assays were analyzed by 2-way ANOVA. **G** The subcutaneous tumors from the BALB/c Nude mice injected LV-Ctrl or LV-*Baiap2l2* MKN45/DDP cells, with DDP treatment (DDP 5 mg/kg once per week). **H** Weight and volume of subcutaneous tumors. Data on subcataneous tumor volume were analyzed by 2-way ANOVA. **I-J** Immunohistochemistry (IHC) staining were performed to detect the expression of BAIAP2L2 in GC tissues of patients resistant or sensitive to Platinum-based treatment. Scale bars for 20 × figures are 100 μm, and those for 40 × figures are 50 μm. The *P* value was calculated with the chi-square test (χ^2)

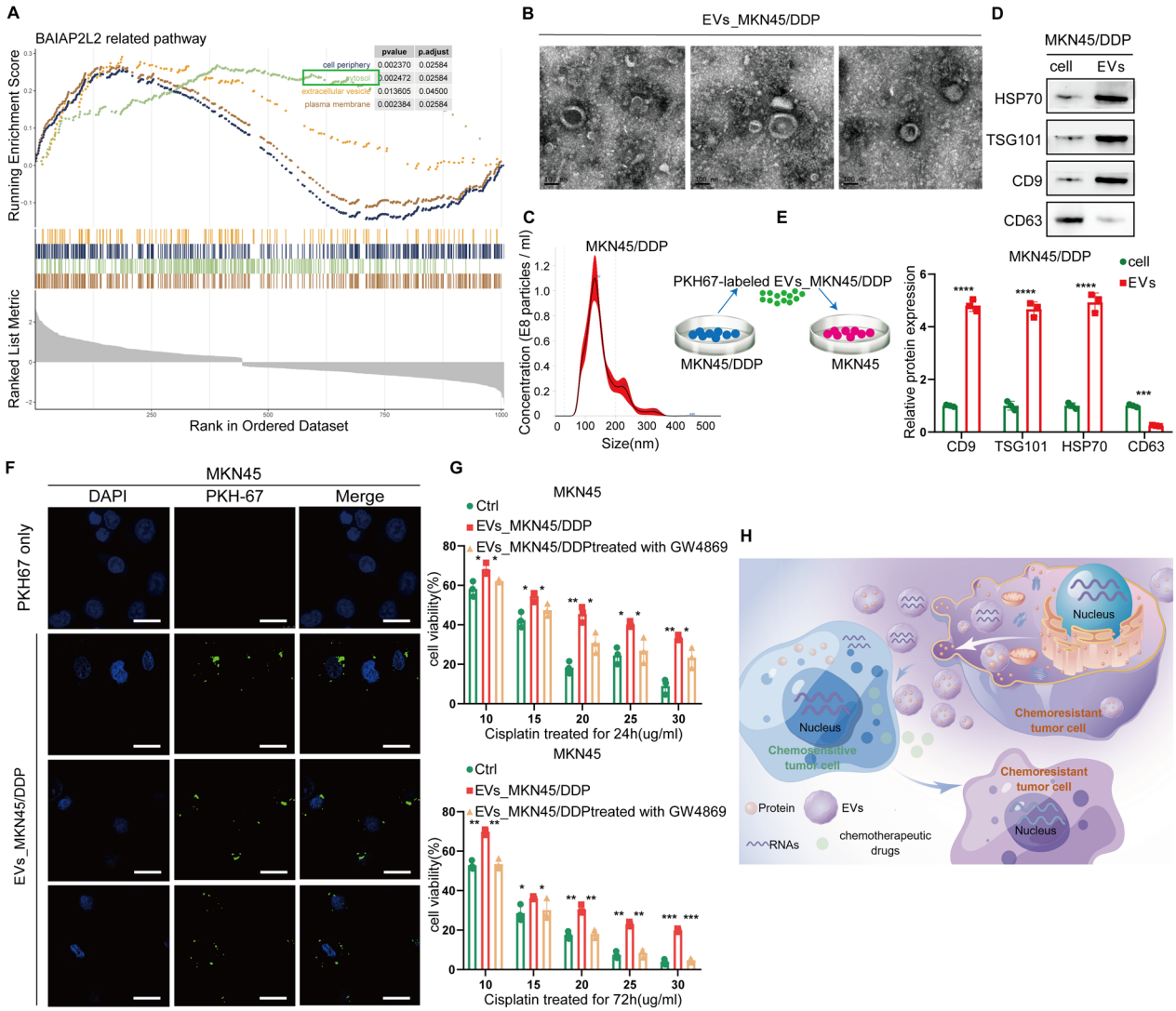

Fig. 3 Chemotherapy resistant GC cells transmit chemotherapy resistance to sensitive cells through EVs. **A** GSEA plot for the mechanism of cisplatin recurrence in gastric cancer that BAIAP2L2 is most likely involved. **B** Representative transmission electron microscope image (scale, 100 nm) of EVs derived from MKN45/DDP cells. **C** Nanoparticle Tracking Analysis (NTA) were performed to show purified EV size (nm). **D** Exosomal markers (HSP70, TSG101, CD9 and CD63) in MKN45/DDP cell proteins and corresponding EVs were analyzed by Western Blot. **E** Flow diagram of EV labeling and co-culture. **F** Immunofluorescence (IF) showed that EVs derived from MKN45/DDP stained with PKH67 fused into sensitive MKN45 cells. Scale bars were 20 μm. **G** CCK-8 were used to explore the effect of EVs_MKN45/DDP. **H** Mechanism overview diagram. The figures and graphical elements were created and compiled using Figdraw (https://www.figdraw.com/)

(See figure on next page.)

Fig. 4 BAIAP2L2 promotes the transfer of chemotherapy resistance from resistant GC cells to sensitive cells through EVs. **A** Representative transmission electron microscope image (scale, 100 nm) of EVs derived from knocked-down or control BAIAP2L2 MKN45/DDP cells. **B** NTA were performed to show the size of purified EVs derived from knocked-down or control BAIAP2L2 MKN45/DDP cells (nm). **C** Flow diagram of EV labeling and co-culture. **D** EVs derived from overexpression or control BAIAP2L2 MKN45/DDP stained with PKH67 fused into sensitive MKN45 cells. **E** EVs markers (HSP70, TSG101, CD9 and CD63) and BAIAP2L2 in knocked-down or control BAIAP2L2 MKN45/DDP cell proteins and corresponding EVs were analyzed by Western Blot. **F** CCK-8 were used to explore the effect of EVs isolated from knocked-down or overexpression BAIAP2L2 MKN45/DDP. **G-H** Top ten molecules select from down-regulated proteins according to logFC in TMT analysis. **I** CCK-8 were used to confirm that ANXA4 could promote chemotherapy resistance

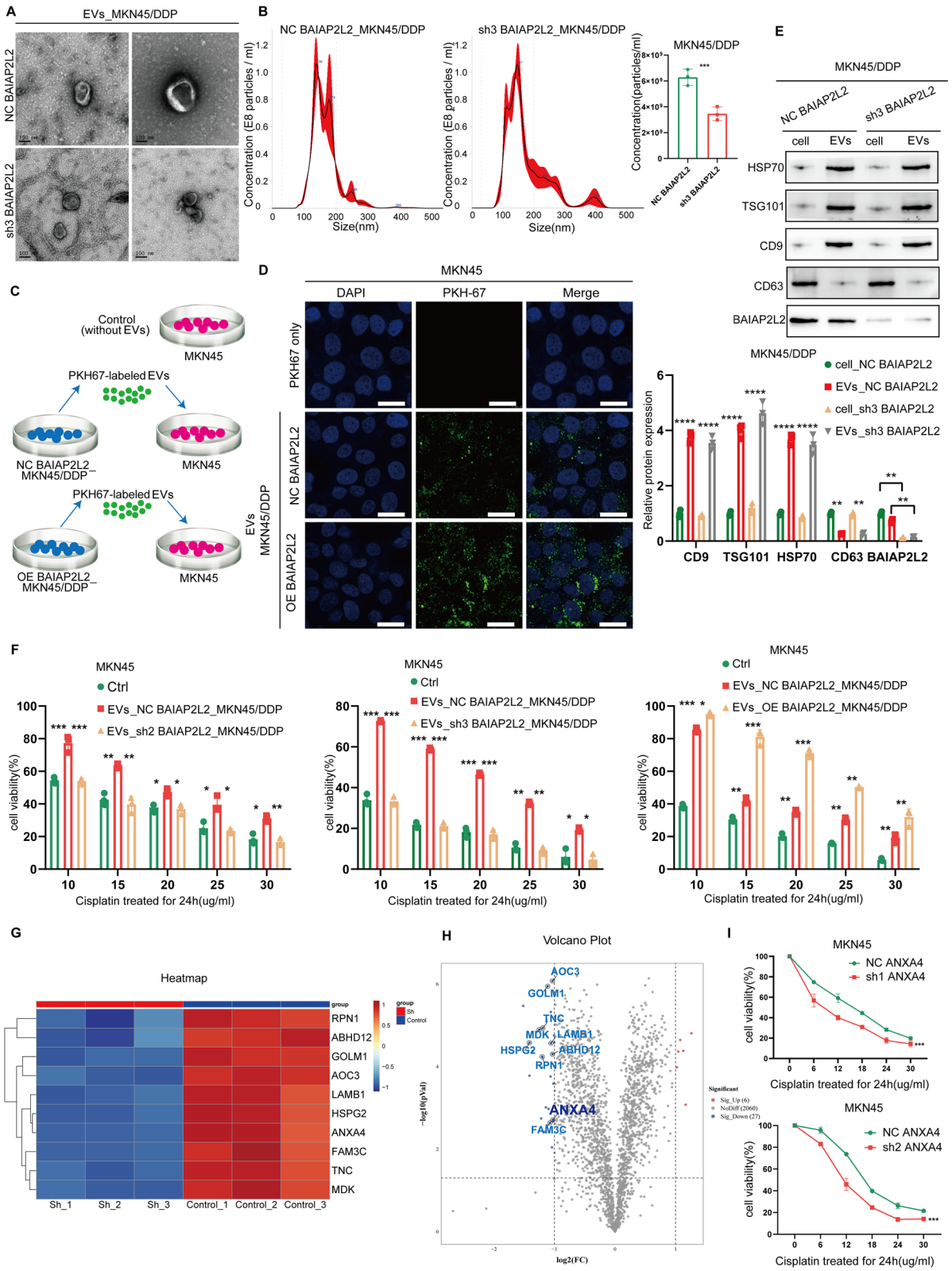

Fig. 4 (See legend on previous page.)

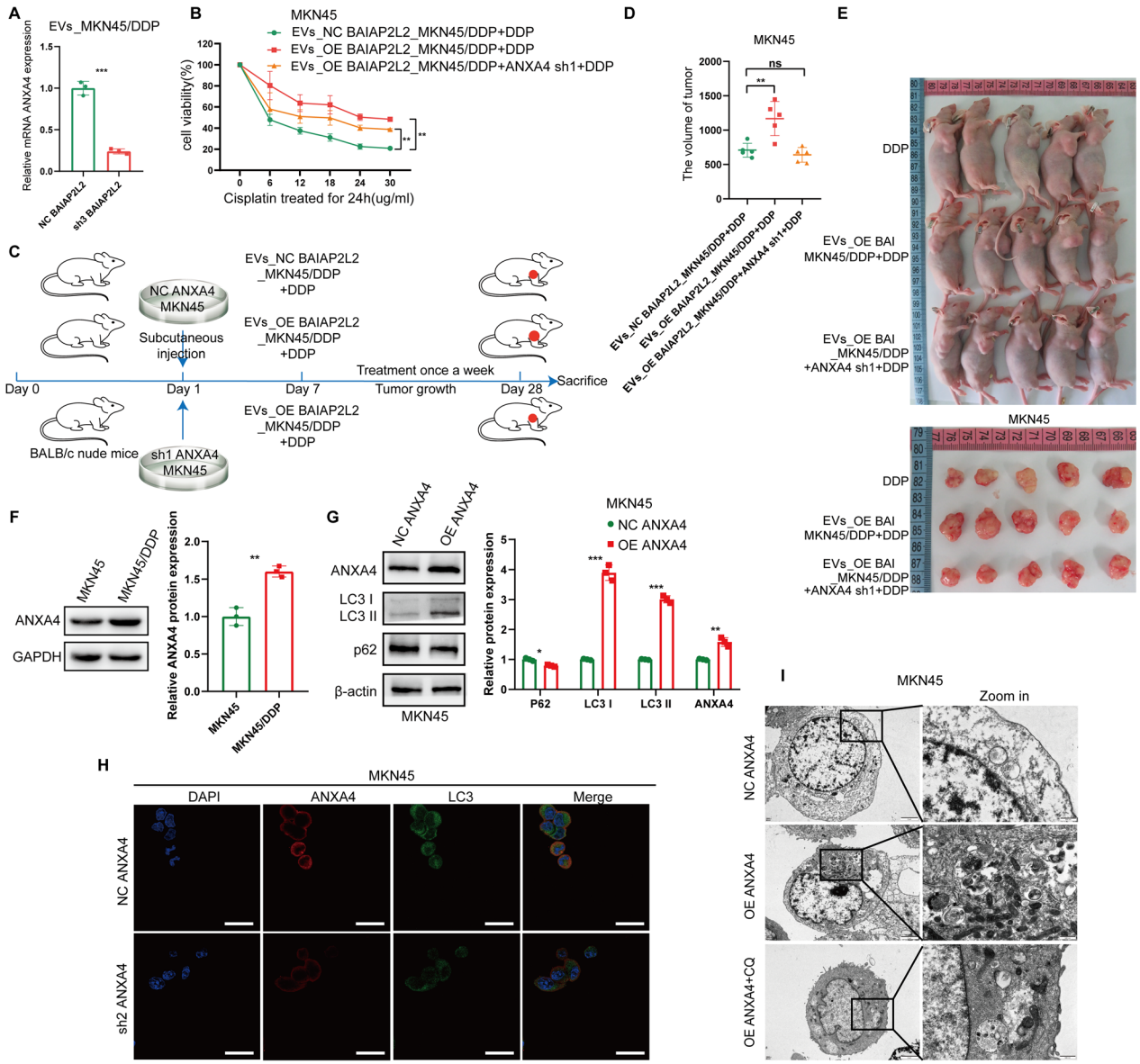

Fig. 5 ANXA4 promotes platinum-based chemical resistance in GC by mediating autophagy. **A** qPCR showed the expression of ANXA4 in EVs from BAIAP2L2 knock-down MKN45/DDP and in the control group. **B** CCK-8 were used to explore the counteraction of pre-knockdown of ANXA4 in MKN45 cells to the effect of EVs isolated from BAIAP2L2 overexpression MKN45/DDP. **C-E** The subcutaneous tumors from the BALB/c Nude mice injected LV-Ctrl or LV-*ANXA4* MKN45 sensitive cells, with DDP treatment (DDP 5 mg/kg once per week), with 20 μg of different EVs (resuspended in 40 μL of PBS) injected through the caudal vein as once per week. **C** Flow diagram of Flow diagram of Subcutaneous tumor model. **D** Volume of subcutaneous tumors. Data on subcataneous tumor volume were analyzed by 2-way ANOVA. J Flow diagram of the subcutaneous tumor xenograft experiment in BALB/c Nude mice. **F** Western Blot showed the expression of ANXA4 in DDP-resistant GC cells and DDP-sensitive cells. **G**, **H** Western Blot and IF showed the expression of LC3 and p62 levels in ANXA4 overexpression MKN45 and the control group. **I** TEM images of ultrastructure microstructure in representative overexpression ANXA4 and control group

isolated from BAIAP2L2 knockdown MKN45/DDP cells significantly increased the sensitivity of MKN45 cells to chemotherapy, while BAIAP2L2 overexpression had the opposite effect, suggesting a regulatory role of BAIAP2L2 in EV-mediated drug resistance. To ensure that these effects were specifically attributed to EV transfer, the negative control for resistance transfer consisted of recipient cells treated with conditioned media from resistant cells depleted of EVs. (Fig. 4F). To confirm which proteins are delivered by BAIAP2L2 to GC-sensitive cells through EVs, we extracted EVs derived from MKN45/DDP cells of the BAIAP2L2 knockdown and control groups,

respectively. We used tandem mass tag (TMT) analysis to detect differential labels, most of which were downregulated in the BAIAP2L2 knockdown group compared to the control group. These downregulated proteins comprised almost all proteins that promoted chemotherapy resistance, which is consistent with our previous experimental results. The top ten molecules selected from downregulated proteins according to logFC were ANXA4, HSPG2, MDK, RPN1, TNC, GOLM1, FAM3C, LAMB1, AOC3, and ABHD12 (Fig. 4G, H). CCK-8 was used to screen for molecules in the EVs that could promote chemotherapy resistance (Fig. 4I and Fig. S2). The CCK-8 assay showed that ANXA4 increased resistance to platinum chemotherapeutics in GC cells (Fig. 4I).

ANXA4 promotes platinum-based chemical resistance in GC by mediating autophagy

ANXA4 promotes autophagy and promotes tumor progression [27, 28]. We hypothesized that ANXA4 promotes chemotherapy resistance in GC cells by regulating autophagy. QPCR showed that the expression of ANXA4 in EVs from BAIAP2L2 knock-down MKN45/DDP cells was significantly lower than that in the control group (Fig. 5A). Moreover, CCK-8 and subcutaneous tumor xenograft experiments in BALB/c Nude mice revealed that co-culture with EVs isolated from BAIAP2L2 overexpressing MKN45/DDP significantly increased the resistance of MKN45 cells to chemotherapy, whereas pre-knockdown of ANXA4 in MKN45 cells counteracted this effect (Fig. 5B–E). Western blotting showed that the expression of ANXA4 in DDP-resistant GC cells was significantly higher than that in DDP-sensitive cells (Fig. 5F). Furthermore, western blotting and IF showed that the overexpression of ANXA4 promoted basic autophagy in MKN45 cells, as determined by LC3 and p62 levels (Fig. 5 G&H). These results confirmed that overexpression ANXA4 resulted in decreased AV counts (Fig. 5 I).

YTHDF1 facilitates BAIAP2L2 translation through m^{6}A modification

We found that traditional RNA regulatory mechanisms were downregulated in the tumor tissues of platinum-based chemotherapy-resistant patients (Fig. 1F). We also used GSEA to confirm the change in classical gene transcription regulation in advance (Fig. 6A), which suggests that other modification mechanisms may be involved in this regulation. M^{6}A modification is one of the most important and common messenger RNA modifications, and using the TIMER database, we found that m^{6}A related proteins, especially reader proteins, were positively correlated with BAIAP2L2, among which YTHDF1 was the most obvious (Fig. S4). YTHDF1 overexpression and knockdown significantly increased or decreased the protein level of BAIAP2L2, but did not affect its mRNA level (Fig. 6B, C and Fig. S3A). Western blotting showed that the expression of YTHDF1 in DDP-resistant GC cells was significantly higher than that in the DDP-sensitive cells (Fig. 6D).The m6A modification status of BAIAP2L2 was assessed using MeRIP-qPCR (Fig. 6E and Fig. S3B). Subsequently, the interaction between YTHDF1 and BAIAP2L2 in MKN45 and MKN45/DDP cells was confirmed using the YTHDF1-specific antibody in RIP-qPCR analysis (Fig. 6F). Furthermore, CCK-8 assay confirmed that YTHDF1 significantly increased the resistance of GC cells to platinum chemotherapeutics (Fig. 6G). IHC staining showed that the expression of YTHDF1 in GC tissues of patients resistant to platinum-based treatment was significantly higher than that in the sensitive group (Fig. 6H, I). We knocked down YTHDF1 in MKN45/DDP cells and performed a subcutaneous tumor xenograft experiment in BALB/c Nude mice. On the day of dissection, the weight and volume of the subcutaneous tumors formed by YTHDF1 knockdown cells were smaller than those formed by control cells (Fig. 6J, K). IHC staining of subcutaneous tumors also confirmed that YTHDF1 knockdown significantly decreased the protein level of BAIAP2L2 (Fig. 6L, M).

(See figure on next page.)

Fig. 6 YTHDF1 facilitates BAIAP2L2 translation through m^{6}A modification. **A** GSEA plot for the pathways associated with the regulation of transcription by RNA polymerase II in drug-resistance group. **B-C** qPCR, western blot and IF (Scale bars were 20 μm) were used to explore the regulation effect of YTHDF1 on BAIAP2L2. **D** Western Blot showed the expression of YTHDF1 in DDP-resistant GC cells and DDP-sensitive cells. **E** Methylated RNA immunoprecipitation of the transcripts of BAIAP2L2 in AGS, MKN45 and MKN45/DDP. **F** YTHDF1 immunoprecipitation assays of BAIAP2L2 transcripts in YTHDF1-bound mRNAs in MKN45 and MKN45/DDP. **G** CCK-8 were used to explore the effect of YTHDF1 on the resistance to platinum chemotherapeutics of GC cells. Data of CCK-8 assays were analyzed by 2-way ANOVA. **H–I** IHC staining were performed to detect the expression of YTHDF1 in GC tissues of patients resistant or sensitive to Platinum-based treatment. Scale bars for 20 × figures are 100 μm, and those for 40 × figures are 50 μm. The *P* value was calculated with the chi-square test (χ^2). **J** The subcutaneous tumors from the BALB/c Nude mice injected LV-Ctrl or LV-*ythdf1* MKN45/DDP cells, with DDP treatment (DDP 5 mg/kg once per week). **K** Weight and volume of subcutaneous tumors. Data on subcataneous tumor volume were analyzed by 2-way ANOVA. **L–M** IHC staining of the subcutaneous tumors was used to confirmed the regulation effect of YTHDF1 on BAIAP2L2.Scale bars for 20 × figures are 100 μm, and those for 40 × figures are 50 μm. The *P* value was calculated with the chi-square test (χ^2)

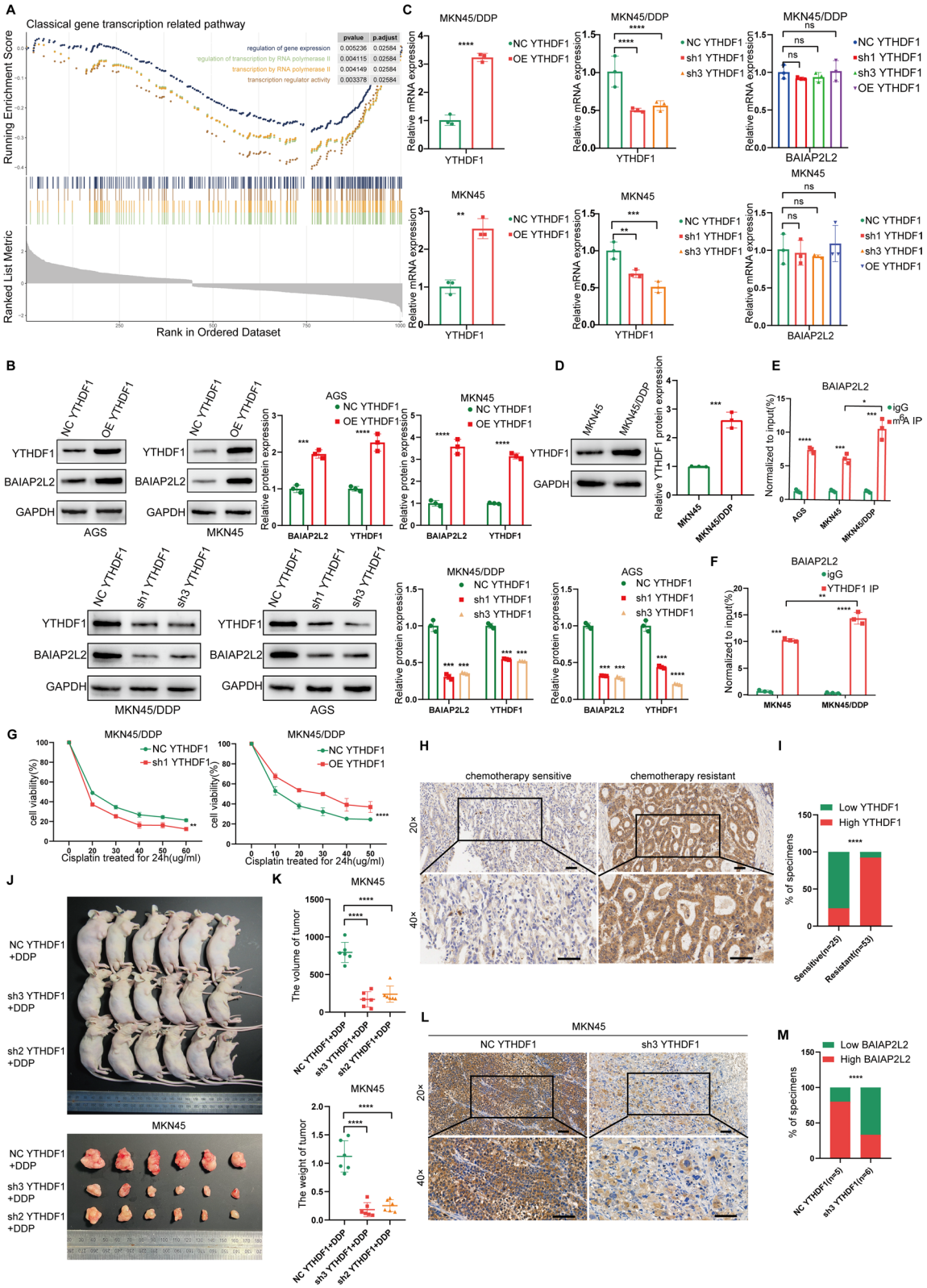

Fig. 6 (See legend on previous page.)

YTHDF1 facilitates ANXA4 translation through m^6A modification.

QPCR showed that BAIAP2L2 and ANXA4 were not affected by their expression levels (Fig. 7A, B). YTHDF1 overexpression and knockdown significantly increased or decreased the protein level of ANXA4 but did not affect its mRNA levels (Fig. 7C–E). Moreover, the interaction between YTHDF1 and ANXA4 in MKN45 and MKN45/DDP cells was confirmed using the YTHDF1-specific antibody in RIP-qPCR analysis (Fig. S5). Subsequently, CCK-8 showed that co-culture with EVs (20 μg/mL) isolated from YTHDF1 overexpression MKN45/DDP significantly increased the resistance of MKN45 cells to chemotherapy, while pre-knockdown of ANXA4 in MKN45 cells counteracted this effect (Fig. 7F). However, CCK-8 and subcutaneous tumor xenograft experiments in BALB/c Nude mice revealed that co-culture with EVs (20 μg/mL) isolated from YTHDF1 overexpression MKN45/DDP significantly increased the resistance of MKN45 cells to chemotherapy, while knockdown of ANXA4 in MKN45/DDP cells did not counteract this effect (Fig. 7G–J).

Discussion

Based on differential expression analysis and cox survival analysis, we identified five genes associated with gastric cancer progression and chemotherapy resistance: BAIAP2L2, TRIM15, TRIM29, KRTCAP3, and GPR35. Previous studies have shown that TRIM15 confers resistance to tyrosine kinase inhibitors in liver cancer cells [29]; TRIM29 plays a crucial role in promoting cisplatin resistance in esophageal squamous cell carcinoma [30], oxaliplatin resistance in colon cancer [31], and cisplatin resistance in ovarian cancer through m6A-YTHDF1-mediated mechanisms [32]; KRTCAP3 has not been reported to be associated with cancer; GPR35 promotes macrophage immune infiltration in gastric cancer tissues [33]; while only BAIAP2L2 has been reported to be associated with gastric cancer, and no studies have yet elucidated its role in drug resistance, thus ensuring logical coherence avoiding limitations in novelty. In the survival curves, BAIAP2L2 was relatively prominent. Moreover, TRIM15, TRIM29, KRTCAP3, and GPR35 did not show as significant a difference as BAIAP2L2 in qPCR results. Therefore, BAIAP2L2 was prioritized for further investigation.

The molecular complexity of GC contributes to its suboptimal clinical response to chemotherapy. In this study, we provide the first evidence that BAIAP2L2 is associated with chemotherapy resistance in GC. We discovered that BAIAP2L2 mediates the transmission of chemotherapy resistance in GC cells by regulating EVs proteins and that YTHDF1 can regulate its expression. These findings reveal that BAIAP2L2 is a biological marker for assessing the response to chemotherapy in GC.

The primary function of BAIAP2L2 was to promote the formation of flat or slightly curved membranes. We first found that chemotherapy resistant GC cells can transmit chemotherapy resistance to sensitive cells through EVs and BAIAP2L2 can regulate EVs. The actin cytoskeleton has been shown to play a key role in vesicle transport at the plasma membrane (PM) by acting as a track for vesicle movement associated with its actin-based motor. Rapid actin polymerization can directly transport intracellular vesicles, and the actin cytoskeleton plays an important role in PM vesicle fusion. Studies have shown that the actin cytoskeleton acts as a physical barrier that needs to be depolymerized to allow vesicles to dock at the PM. Actin polymerization is required to facilitate vesicle-membrane fusion, where vesicles are released into the extracellular environment after late endosome/polyvesicle (MVB) fusion with the plasma membrane [26]. Transport of MVB to the plasma membrane depends on its interactions with actin and the microtubule cytoskeleton [27, 28], whereas The I-BAR family of proteins is a well-known actin-cytoskeletal adapter [34]. However, this finding has only been investigated in GC, and the presence of this biological phenomenon in normal cells and other tumors remains to be explored.

At present, most studies on tumor EVs have focused on RNA in EVs [11, 13, 14]. Using tandem mass tag (TMT) analysis, we found that BAIAP2L2 delivers the protein ANXA4 to GC-sensitive cells through EVs, leading to the

(See figure on next page.)

Fig. 7 YTHDF1 facilitates ANXA4 translation through m^6A modification. **A-B** QPCR was used to explore the interaction between BAIAP2L2 and ANXA4. **D**, **E** QPCR and western blot were used to explore the regulation effect of YTHDF1 on ANXA4. **F** CCK-8 were used to explore the counteraction of knockdown of ANXA4 in MKN45 cells to the effect of EVs isolated from YTHDF1 overexpression MKN45/DDP. **G** CCK-8 were used to explore the counteraction of knockdown of ANXA4 in YTHDF1 overexpression MKN45/DDP cells to the effect of MKN45. **H** Flow diagram of Flow diagram of Subcutaneous tumor model. **I** The subcutaneous tumors from the BALB/c Nude mice injected MKN45 sensitive cells, with DDP treatment (DDP 5 mg/kg once per week), with 20 μg of different EVs (resuspended in 40 μL of PBS) injected through the caudal vein as once per week. **J** Volume of subcutaneous tumors. Data on subcataneous tumor volume were analyzed by 2-way ANOVA. J Flow diagram of the subcutaneous tumor xenograft experiment in BALB/c Nude mice. **K** Mechanism diagram. The figures and graphical elements were created and compiled using Figdraw (https://www.figdraw.com/)

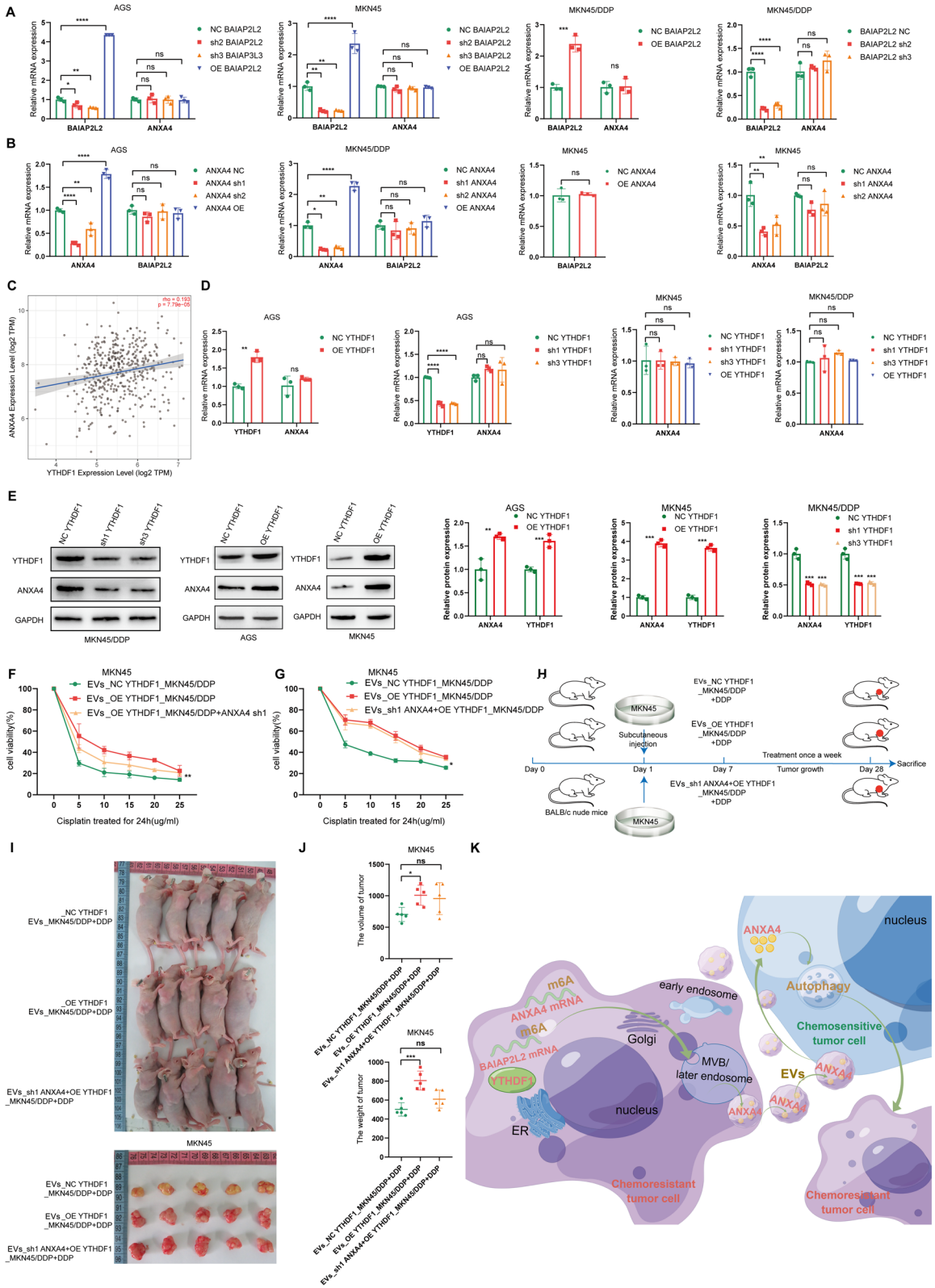

Fig. 7 (See legend on previous page.)

transmission of chemotherapy resistance in GC. Moreover, we found that ANXA4 promotes platinum-based chemical resistance in GC by mediating autophagy.

Conclusions

We found that traditional RNA regulatory mechanisms were downregulated in the tumor tissues of patients with platinum-based chemotherapy resistance, suggesting that other modification mechanisms may be involved in this regulation. M^6A modification is one of the most important and common messenger RNA modifications; using the TIMER database analysis and a series of experiments, we found that YTHDF1 facilitates BAIAP2L2 translation through m6A modification (Fig. 7K). These results confirmed that the high expression of BAIAP2L2 in GC-resistant cells is due to the regulation of YTHDF1. Furthermore, we found that YTHDF1 can also facilitate ANXA4 translation in a similar way.

Abbreviations

GC	Gastric Cancer
BAIAP2L2	Brain-specific Angiogenesis Inhibitor 1-associated Protein-2-like Protein 2
MKN45/DDP	MKN45/DDP Cisplatin resistant cells
TMT	Tandem Mass Tag
YTHDF1	YTH Domain-containing Family Protein1
RIP-qPCR	RNA Immunoprecipitation-qPCR
MeRIP-qPCR	Methylated RNA Immunoprecipitation; EVs;
M6A	N6-methyladenosine;
IHC	Immunohistochemistry
IF	Immunofluorescence
WB	Western Blot
STR	Short Tandem Repeat
NTA	Nanoparticle Tracking Analysis
TCGA	The Cancer Genome Atlas
DEGs	Differentially Expressed Genes
PAGs	Genes Associated with Prognosis
KEGG	Kyoto Encyclopedia of Genes and Genomes
ORA	Over-representation Analysis
GSEA	Gene Set Enrichment Analysis

Supplementary Information

The online version contains supplementary material available at https://doi.org/10.1186/s12967-025-06340-6.

Supplementary material 1

Supplementary material 2

Supplementary material 3

Acknowledgements

Not applicable

Author contributions

L.Z. and J.Y. designed the study, and prepared the manuscript. Y. L. and X.C. performed experiments. Y.Z. performed statistical analyses. X.Z. assisted with tissue sample collection. H.X. performed the data analysis and interpretation. All the authors approved the final version of the manuscript.

Funding

Guangzhou Basic and Applied Basic Research Foundation (2024A04J6605), Beijing Science and Technology Innovation Medical Development Foundation (KC2023-JX-0186-FQ043) and President Foundation of Nanfang Hospital, Southern Medical University (2022A008).

Availability of data and materials

The datasets generated and/or analyzed during the current study are not publicly available but are available from the corresponding author upon reasonable request.

Declarations

Ethics approval and consent to participate

All experiments involving patients were approved by the Ethics Committee of Nanfang Hospital, Southern Medical University and complied with the Declaration of Helsinki (No. NFEC-2023-545). Informed consent was not required because the data were analyzed anonymously. All animal experiments involved ethical and humane treatment under license from the Guangdong Provincial Bureau of Science and complied with Declaration of Basel.

Consent for publication

Not applicable.

Competing interests

The authors have declared that no competing interests exists.

Author details

[1]Department of Pathology, Nanfang Hospital, Southern Medical University, Guangzhou, China. [2]Department of Pathology &, Guangdong Province Key Laboratory of Molecular Tumor Pathology, School of Basic Medical Sciences, Southern Medical University, Guangzhou, China. [3]Department of General Surgery, Nanfang Hospital, Southern Medical University, Guangzhou, China. [4]Department of Gastroenterology, Chinese Academy of Medical Sciences, Peking Union Medical College Hospital, Beijing, China.

Received: 14 October 2024 Accepted: 1 March 2025
Published online: 13 March 2025

References

1. Sung H, Ferlay J, Siegel RL, Laversanne M, Soerjomataram I, Jemal A, Bray F. Global cancer statistics 2020: GLOBOCAN estimates of incidence and mortality worldwide for 36 cancers in 185 countries. Cancer J Clin. 2021;71:209–49.
2. Joshi SS, Badgwell BD. Current treatment and recent progress in gastric cancer. Cancer J Clin. 2021;71:264–79.
3. Janjigian YY, Kawazoe A, Yañez P, Li N, Lonardi S, Kolesnik O, Barajas O, Bai Y, Shen L, Tang Y, Wyrwicz LS, Xu J, Shitara K, Qin S, Van Cutsem E, Tabernero J, Li L, Shah S, Bhagia P, Chung HC. The KEYNOTE-811 trial of dual PD-1 and HER2 blockade in HER2-positive gastric cancer. Nature. 2021;600:727–30.
4. Janjigian YY, Shitara K, Moehler M, Garrido M, Salman P, Shen L, Wyrwicz L, Yamaguchi K, Skoczylas T, Campos Bragagnoli A, Liu T, Schenker M, Yanez P, Tehfe M, Kowalyszyn R, Karamouzis MV, Bruges R, Zander T, Pazo-Cid R, Hitre E, Feeney K, Cleary JM, Poulart V, Cullen D, Lei M, Xiao H, Kondo K, Li M, Ajani JA. First-line nivolumab plus chemotherapy versus chemotherapy alone for advanced gastric, gastro-oesophageal junction, and oesophageal adenocarcinoma (CheckMate 649): a randomised, open-label, phase 3 trial. Lancet. 2021;398:27–40.
5. Carman PJ, Dominguez R. BAR domain proteins—a linkage between cellular membranes, signaling pathways, and the actin cytoskeleton. Biophys Rev. 2018;10:1587–604.
6. Takemura K, Hanawa-Suetsugu K, Suetsugu S, Kitao A. Salt bridge formation between the I-BAR domain and lipids increases lipid density and membrane curvature. Sci Rep. 2017;7:6808.
7. Xu L, Du H, Zhang Q, Wang C, Yan L, Tian G, Fu X. BAI1-associated protein 2-like 2 is a potential biomarker in lung cancer. Oncol Rep. 2019;41:1304–12.
8. Guo H, Peng J, Hu J, Chang S, Liu H, Luo H, Chen X, Tang H, Chen Y. BAIAP2L2 promotes the proliferation, migration and invasion of

osteosarcoma associated with the Wnt/β-catenin pathway. J Bone Oncol. 2021;31: 100393.
9. Liu J, Shangguan Y, Sun J, Cong W, Xie Y. BAIAP2L2 promotes the progression of gastric cancer via AKT/mTOR and Wnt3a/β-catenin signaling pathways. Biomed Pharmacother. 2020;129: 110414.
10. Kalluri R, LeBleu VS. The biology, function, and biomedical applications of EVs. Science. 2020;367:eaau6977.
11. Wang X, Zhang H, Bai M, Ning T, Ge S, Deng T, Liu R, Zhang L, Ying G, Ba Y. EVs serve as nanoparticles to deliver anti-miR-214 to reverse chemoresistance to cisplatin in gastric cancer. Mol Ther. 2018;26:774–83.
12. Fan J, Wei Q, Koay EJ, Liu Y, Ning B, Bernard PW, Zhang N, Han H, Katz MH, Zhao Z, Hu Y. Chemoresistance transmission via exosome-mediated EphA2 transfer in pancreatic cancer. Theranostics. 2018;8:5986–94.
13. Guo J, Zhong X, Tan Q, Yang S, Liao J, Zhuge J, Hong Z, Deng Q, Zuo Q. miR-301a-3p induced by endoplasmic reticulum stress mediates the occurrence and transmission of trastuzumab resistance in HER2-positive gastric cancer. Cell Death Dis. 2021;12:696.
14. Lin L, Yang L, Zeng Q, Wang L, Chen M, Zhao Z, Ye G, Luo Q, Lv P, Guo Q, Li B, Cai J, Cai W. Tumor-originated exosomal lncUEGC1 as a circulating biomarker for early-stage gastric cancer. Mol Cancer. 2018;17:84.
15. Yousafzai NA, Wang H, Wang Z, Zhu Y, Zhu L, Jin H, Wang X. Exosome mediated multidrug resistance in cancer. Am J Cancer Res. 2018;8:2210.
16. Kang M, Kim S, Ko J. Roles of CD133 in microvesicle formation and oncoprotein trafficking in colon cancer. FASEB J. 2019;33:4248–60.
17. Pi J, Wang W, Ji M, Wang X, Wei X, Jin J, Liu T, Qiang J, Qi Z, Li F. YTHDF1 promotes gastric carcinogenesis by controlling translation of FZD7. Can Res. 2021;81:2651–65.
18. Yue B, Song C, Yang L, Cui R, Cheng X, Zhang Z, Zhao G. METTL3-mediated N6-methyladenosine modification is critical for epithelial-mesenchymal transition and metastasis of gastric cancer. Mol Cancer. 2019;18:1–15.
19. Bai X, Wong CC, Pan Y, Chen H, Liu W, Zhai J, Kang W, Shi Y, Yamamoto M, Tsukamoto T. Loss of YTHDF1 in gastric tumors restores sensitivity to antitumor immunity by recruiting mature dendritic cells. J Immunother Cancer. 2022;10:e003663.
20. Li R, Zhou R, Wang H, Li W, Pan M, Yao X, Zhan W, Yang S, Xu L, Ding Y. Gut microbiota-stimulated cathepsin K secretion mediates TLR4-dependent M2 macrophage polarization and promotes tumor metastasis in colorectal cancer. Cell Death Differ. 2019;26:2447–63.
21. Nguyen VVT, Ye S, Gkouzioti V, van Wolferen ME, Yengej FY, Melkert D, Siti S, de Jong B, Besseling PJ, Spee B, van der Laan LJW, Horland R, Verhaar MC, van Balkom BWM. A human kidney and liver organoid-based multi-organ-on-a-chip model to study the therapeutic effects and biodistribution of mesenchymal stromal cell-derived extracellular vesicles. J Extracell Vesic. 2022;11:12280.
22. Tang Z, Kang B, Li C, Chen T, Zhang Z. GEPIA2: an enhanced web server for large-scale expression profiling and interactive analysis. Nucleic Acids Res. 2019;47:W556–60.
23. Kanehisa M, Furumichi M, Sato Y, Ishiguro-Watanabe M, Tanabe M. KEGG: integrating viruses and cellular organisms. Nucleic Acids Res. 2021;49:D545–51.
24. Resource GO, Years and still GOing strong| nucleic acids research| Oxford Academic.
25. Wu T, Hu E, Xu S, Chen M, Guo P, Dai Z, Feng T, Zhou L, Tang W, Zhan LI. clusterProfiler 4.0: a universal enrichment tool for interpreting omics data. Innovation. 2021;2:100141.
26. Hessvik NP, Llorente A. Current knowledge on exosome biogenesis and release. Cell Mol Life Sci. 2018;75:193–208.
27. Villarroya-Beltri C, Baixauli F, Gutiérrez-Vázquez C, Sánchez-Madrid F, Mittelbrunn M, Sorting it out: regulation of exosome loading, 2014, pp. 3–13
28. Hoshino D, Kirkbride KC, Costello K, Clark ES, Sinha S, Grega-Larson N, Tyska MJ, Weaver AM. Exosome secretion is enhanced by invadopodia and drives invasive behavior. Cell Rep. 2013;5:1159–68.
29. Yang C, Jin X, Liu X, Wu G, Yang W, Pang B, Jiang J, Liao D, Zhang Y. TRIM15 forms a regulatory loop with the AKT/FOXO1 axis and LASP1 to modulate the sensitivity of HCC cells to TKIs. Cell Death Dis. 2023;14:47.
30. Nan Y, Luo Q, Wu X, Chang W, Zhao P, Liu S, Liu Z. HCP5 prevents ubiquitination-mediated UTP3 degradation to inhibit apoptosis by activating c-Myc transcriptional activity. Mol Ther. 2023;31:552–68.
31. Lei G, Liu S, Yang X, He C. TRIM29 reverses oxaliplatin resistance of P53 mutant colon cancer cell. Can J Gastroenterol Hepatol. 2021;2021:8870907.
32. Hao L, Wang J, Liu B, Yan J, Li C, Jiang J, Zhao F, Qiao H, Wang H. m6A-YTHDF1-mediated TRIM29 upregulation facilitates the stem cell-like phenotype of cisplatin-resistant ovarian cancer cells. Biochim et Biophys Acta. 2021;1868:118878.
33. Shu C, Wang C, Chen S, Huang X, Cui J, Li W, Xu B. ERR-activated GPR35 promotes immune infiltration level of macrophages in gastric cancer tissues. Cell Death Dis. 2022;8:444.
34. Chen Z, Shi Z, Baumgart T. Regulation of membrane-shape transitions induced by I-BAR domains. Biophys J. 2015;109:298–307.

Publisher's Note